

# Zero-threshold correlated-photon laser with a single trapped atom in a bimodal cavity

Anushree Dey,<sup>1</sup> Arpita Pal,<sup>2,\*</sup> Subhasish Dutta Gupta,<sup>3,4,5,†</sup> and Bimalendu Deb<sup>1,‡</sup>

<sup>1</sup>*School of Physical Sciences, Indian Association for the Cultivation of Science, Jadavpur, Kolkata 700032, India.*

<sup>2</sup>*Centre for Quantum Engineering, Research and Education, TCG CREST, Salt Lake, Kolkata 700091, India.*

<sup>3</sup>*Department of Physical Sciences, Indian Institute of Science Education and Research (IISER) Kolkata. Mohanpur 741246, India.*

<sup>4</sup>*Tata Centre for Interdisciplinary Sciences, TIFRH, Hyderabad 500107, India.*

<sup>5</sup>*School of Physics, University of Hyderabad, Hyderabad 500046, India.*

## Abstract

We demonstrate theoretically the feasibility of correlated photon-pair generation with vanishing threshold in a bimodal cavity setup that uses a single  $V$ -type three level atom pumped by dual incoherent sources and driven by two coherent fields. The photon-pair is shown to be entangled only for low levels of the incoherent pump and owes its origin solely to the coherent drives. The steady-state features as regards the average photon numbers, intra- and inter- mode Hanbury-Brown-Twiss (HBT) correlation functions are studied in detail. We show that the dual incoherent pumping with no coherent drive can lead to amplification of the cavity fields with strong inter-mode antibunching but no entanglement. We analyse our results in terms of an interplay between coherent and incoherent processes involving cavity-dressed states. Both the inter- and intra-mode HBT functions exhibit temporal oscillations in the strong-coupling cavity QED regime. Our theoretical scheme for the generation of nonclassical and entangled photon pairs may find interesting applications in quantum metrology and quantum information science.

---

\* Present address: Department of Optics, Palacký University, 17. listopadu 1192/12, 771 46 Olomouc, Czech Republic.

† [sdghyderabad@gmail.com](mailto:sdghyderabad@gmail.com)

‡ [msbd@iacs.res.in](mailto:msbd@iacs.res.in)

## I. INTRODUCTION

Over the years, cavity quantum electrodynamics (CQED) [1–3] where atoms interact with quantized electromagnetic fields have emerged as an excellent platform for engineering entanglement [4, 5], photon blockade [6–8], generation of quantum light [9] and a variety of quantum correlations [10, 11]. Antibunching and entanglement are a crucial resource for quantum information processing, metrology and quantum teleportation [12, 13]. In particular, correlated or entangled photons are essential for photon-based quantum metrology and quantum technology [14–19]. One of the important sources of correlated photons used for a variety of fundamental studies over the years is optical parametric oscillator (OPO) [20–25]. However, the generation of correlated photons by an OPO is probabilistic. In recent times, several theoretical proposals for generating nonclassical or entangled radiation fields by coherently driving multilevel atoms inside a cavity have been put forward [26–28]. Lasing into a single-mode cavity field due to coherent as well as incoherent pumping of multi-level atoms in strong-coupling CQED regime has also been studied [29]. Although, with the currently available conventional laser technology, it is possible to produce extremely narrow-band and high-quality single-mode coherent light sources there hardly exists any standard technique to create a laser source that can deliver entangled or non-classically correlated photons on demand.

A one-atom laser using CQED was theoretically conceived three decades ago [30]. Since then several theoretical as well as experimental studies [31–38] on single-atom CQED laser have been carried out. The steady-state properties of an incoherently pumped single-atom in a single-mode cavity reveal vanishing threshold for lasing action of the cavity mode with interesting atom-photon and photon-photon correlations [35]. A laser with a single trapped ion inside a high-Q cavity was theoretically proposed by Meyer, Briegel and Walther [36] about two decades ago. 1980s and 1990s had witnessed a lot of progress in the development of micromaser [39–42] that uses a mono-energetic beam of Rydberg atoms passing through a high-Q cavity one by one. An optical analog of micromaser, namely microlaser had been realized in the 90s [43, 44]. Although a micromaser or microlaser makes use of the strong atom-cavity interactions of single atoms, it is not truly a one-atom maser or laser as it results from the cumulative effect of interactions of a beam of atoms with the cavity. The recent advancement of trapping and cooling of single atoms and ions opens new prospects for developing a microscopic laser with a single trapped atom inside a high-Q cavity for controlled generation of nonclassical light. In this context, McKeever *et. al.* [37, 38]

had experimentally demonstrated lasing with a single trapped atom in the strong-coupling CQED regime in 2003. A one-atom CQED laser is fundamentally different from a standard laser in many respects. First, it can operate at vanishingly small or zero threshold. Second, its frequency depends on the atom-cavity coupling. Third, it can be operated with a single trapped atom at a few photon levels enabling substantial microscopic control over the output signal amplitude and photon statistics. Fourth, as shown in Ref. [37], it can produce antibunched light which is nonclassical.

Here we propose a model for a single-atom threshold-less bimodal correlated-photon laser (CPL) based on strong-coupling CQED. Our proposed laser system is schematically shown in Fig. 1. It may consist of a pair of crossed cavities or a bimodal cavity, a single trapped  $V$ -type three-level atom inside the bimodal cavity or at the symmetry point of the crossed cavities, two incoherent pumps and two lasers to drive the two atomic transitions. The two excited levels of the atom are incoherently pumped by external sources while a pair of coherent drives (lasers) couple the atomic ground state with the two excited states. The incoherent pumping leads to the amplification of the two cavity modes while coherent driving creates entanglement between the two cavity modes. Even without coherent driving but with dual incoherent pumping, the system produces inter-mode photon antibunching without any photon-photon entanglement. This nonclassical correlation can be attributed to an interplay between the coherent Rabi dynamics due to the cavity fields and the dual incoherent pumping. Only dual incoherent pumping of a  $V$ -type three-level system in free space can not produce any excited-state atomic coherence unless the two transition dipole moments are non-orthogonal [45]. Since all three levels of a  $V$ -type three-level atom have different angular momenta, the two transition dipole moments are orthogonal. However, classical coherent fields or quantized cavity fields can produce the excited-state coherence. We interpret our results in terms of the transitions and coherence between the atom-field dressed states. The origin of the photon-photon entanglement lies in the dressing of the cavity-dressed states by the external coherent fields. When the photons are emitted from such doubly dressed states, they carry forward the nonclassical properties of the dressed states in the form of inter-mode photon-photon entanglement. Our results show that when the atom is driven by external coherent drives in the absence of incoherent pumping or in the presence of small incoherent pumping, lasing in the two cavity modes can happen without any inversion due to the atomic coherence. We also show threshold-less lasing behavior with manifestly nonclassical inter-mode correlation. We find that the entanglement is strongly quenched as we slightly increase the strength of the incoherent pump in the presence of fixed coherent drives.

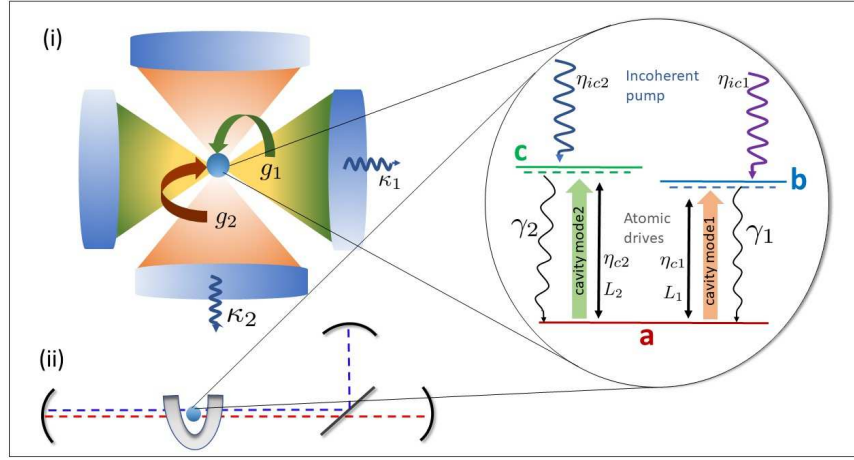


FIG. 1. A schematic diagram showing a single trapped V-type three-level atom interacting with two cavity modes either in a crossed cavity (i) or a doubly-resonant cavity (ii) setup. The zoomed view shows the atomic level diagram with  $a$ ,  $b$  and  $c$  denoting the three atomic levels and the arrows indicate various transition pathways. The cavity modes 1 and 2 couple the lowest level  $a$  to the two upper levels  $b$  and  $c$ , respectively. Here  $\eta_{ic1}$  and  $\eta_{ic2}$  represent two incoherent pumping rates while  $\eta_{c1}$  and  $\eta_{c2}$  are the coherent coupling rates due to laser fields  $L_1$  and  $L_2$  that drive the corresponding atomic transitions.  $\gamma_1$  and  $\gamma_2$  are the atomic decay rates for the transitions  $b \rightarrow a$  and  $c \rightarrow a$ , respectively; while  $\kappa_1$  and  $\kappa_2$  are the cavity decay rates for the modes 1 and 2, respectively.

The paper is organised in the following way: we present theoretical formulation of our problem in Sec. II. We discuss and analyse our results in Sec. III. The paper is concluded in Sec. IV.

## II. THEORETICAL FORMULATION

We consider a trapped V-type three-level atom either at the intersection of a pair of crossed cavities as schematically shown Fig. 1 (i) or in a doubly-resonant cavity setup as shown in Fig. 1 (ii). Here  $a$  denotes the ground state, and  $b$  and  $c$  represent the two excited states which may be degenerate or quasi-degenerate. The two cavity modes 1 and 2 are tuned to the transitions  $a \rightarrow b$  and  $a \rightarrow c$ , respectively. The two excited levels  $b$  and  $c$  are pumped by dual incoherent sources while the two atomic transitions may be driven by two classical laser fields as depicted in Fig. 1.

## A. Hamiltonian

The Hamiltonian for this system is

$$\mathcal{H} = \mathcal{H}_0 + \mathcal{H}_{int} + \mathcal{H}_{drive} , \quad (1)$$

where  $\mathcal{H}_0 = \hbar\omega_b |b\rangle\langle b| + \hbar\omega_c |c\rangle\langle c| + \hbar\omega_1 a_1^\dagger a_1 + \hbar\omega_2 a_2^\dagger a_2$  is the free Hamiltonian with  $\omega_b$  and  $\omega_c$  being the respective atomic transition frequencies. We choose the energy of the lowest level  $a$  to be zero. Here  $a_i(a_i^\dagger)$  denotes the annihilation (creation) operator of the  $i$ -th ( $=1,2$ ) cavity mode. Under electric-dipole and rotating-wave approximation (RWA), the interaction Hamiltonian  $\mathcal{H}_{int}$  can be written as

$$\mathcal{H}_{int} = \hbar \left( g_1 a_1 \sigma_1^\dagger + g_2 a_2 \sigma_2^\dagger \right) + \text{H.c.} , \quad (2)$$

where  $g_1$  and  $g_2$  are the atom-cavity coupling constants that depend on dipole moment and the respective transition field amplitude.  $\sigma_1^\dagger = |b\rangle\langle a|$  and  $\sigma_2^\dagger = |c\rangle\langle a|$  represent the atomic raising operators and the corresponding lowering operators are  $\sigma_1 = |a\rangle\langle b|$  and  $\sigma_2 = |a\rangle\langle c|$ , respectively. Here the Hamiltonian corresponding to the driving of the atomic transitions by two classical fields is given by

$$\mathcal{H}_{drive} = \hbar\eta_{c1}\sigma_1 e^{i\omega_{L1}t} + \hbar\eta_{c2}\sigma_2 e^{i\omega_{L2}t} + \text{H.c.} , \quad (3)$$

where  $\eta_{c1}$  and  $\eta_{c2}$  are the laser-atom coupling constants. In the rotating reference frame of the laser frequencies, the Hamiltonian reads as

$$\begin{aligned} \mathcal{H} = & \hbar \left( \Delta_b |b\rangle\langle b| + \Delta_c |c\rangle\langle c| + \delta_{1L} a_1^\dagger a_1 + \delta_{2L} a_2^\dagger a_2 \right) + \mathcal{H}_{int} \\ & + \hbar \left[ \eta_{c1} \left( \sigma_1 + \sigma_1^\dagger \right) + \eta_{c2} \left( \sigma_2 + \sigma_2^\dagger \right) \right] , \end{aligned} \quad (4)$$

where the detuning parameters are  $\Delta_b = \omega_b - \omega_{L1}$ ,  $\Delta_c = \omega_c - \omega_{L2}$ ,  $\delta_{1L} = \omega_1 - \omega_{L1}$  and  $\delta_{2L} = \omega_2 - \omega_{L2}$ . Here  $\omega_{L1}$  and  $\omega_{L2}$  are the frequencies of  $L_1$  and  $L_2$  lasers. The detuning of the two cavity fields are denoted by  $\delta_1 = \omega_1 - \omega_b$  and  $\delta_2 = \omega_2 - \omega_c$ .

## B. Dressed-states

In the absence of all incoherent processes, one can develop a dressed state description of the driven three-level atom interacting with two cavity modes. Dressed state picture of a CQED problem helps to gain insight into the physical processes underlying the relevant quantum dynamics,

particularly in the strong-coupling regime. We use the two-mode Fock basis  $|n_1, n_2\rangle$  for the two cavity fields, where  $n_1 = 0, 1, 2, \dots, \infty$  and  $n_2 = 0, 1, 2, \dots, \infty$  denote the number of photons in the mode 1 and 2, respectively. One can construct three bare basis states  $|a, n_1, n_2\rangle$ ,  $|b, n_1 - 1, n_2\rangle$ , and  $|c, n_1, n_2 - 1\rangle$  which will be involved in the closed coherent quantum dynamics in the absence of all incoherent processes and couplings to the classical drives.

Defining the excitation number operators  $N_1 = a_1^\dagger a_1 + |b\rangle\langle b|$  and  $N_2 = a_2^\dagger a_2 + |c\rangle\langle c|$  and applying the unitary transformation  $\hat{U}(t) = \exp[-i(\omega_1 N_1 + \omega_2 N_2)t]$  [46], one can obtain the following effective Hamiltonian in the absence of the lasers

$$\tilde{H} = -\delta_1 |b\rangle\langle b| - \delta_2 |c\rangle\langle c| + \mathcal{H}_{int}. \quad (5)$$

If the two cavity fields are tuned to the two-photon resonance  $\delta_1 = \delta_2 = \delta$ , then the eigenvalues of  $\tilde{H}$  are  $\tilde{E}_0 = -\delta$  and  $\tilde{E}_\pm = -\frac{\delta}{2} \pm \frac{1}{2}\sqrt{\delta^2 + 4(n_1 g_1^2 + n_2 g_2^2)}$ . For limited Fock states, the characteristic eigenvalue and eigenstate analysis can be found elsewhere [47].

The eigenstate  $|\psi_0(n_1, n_2)\rangle$  corresponding to the eigenvalue  $\tilde{E}_0$  is given by

$$|\psi_0(n_1, n_2)\rangle = \frac{1}{\sqrt{g_2^2 n_2 + g_1^2 n_1}} [g_1 \sqrt{n_1} |c, n_1, n_2 - 1\rangle - g_2 \sqrt{n_2} |b, n_1 - 1, n_2\rangle]. \quad (6)$$

which is a coherent superposition of the two atom-field joint states involving only the two atomic excited states. It results from the destructive quantum interference between the two cavity field-induced transition pathways  $|b, n_1 - 1, n_2\rangle \longleftrightarrow |a, n_1, n_2\rangle$  and  $|c, n_1, n_2 - 1\rangle \longleftrightarrow |a, n_1, n_2\rangle$  connecting the two joint atom-field excited states to the joint atom-field state with the atom being in the ground state. This is an excited dark state due to the quantized cavity fields. The dark-state resonance and associated phenomena such as coherent population trapping and electromagnetically induced transparency (EIT) are well-known for a Lambda-type three level system interacting with two classical coherent fields. In a recent work, Rempe's group [9] has experimentally demonstrated the generation of single-mode quantum light utilizing the dark state of a coherently driven  $\Lambda$ -type three-level atom inside a single-mode cavity. However, for a  $V$ -type three-level system, the dark state resonance and associated effects are qualitatively different [48]. The excited-state coherence in  $V$ -type three-level atoms driven by classical coherent fields may lead to transient coherent population trapping [49], quantum beat and correlated two-mode lasers as shown by Scully's group [50–53].

The other two dressed states corresponding to the eigenvalues  $E_\pm$  are coherent superposition of all three bare states. For  $\delta = 0$ , these two dressed states can be expressed as

$$\begin{aligned}
|\psi_{\pm}(n_1, n_2)\rangle &= \frac{1}{\sqrt{2}} |a, n_1, n_2\rangle \pm \frac{1}{\sqrt{2(g_2^2 n_2 + g_1^2 n_1)}} \\
&\times [g_2 \sqrt{n_2} |c, n_1, n_2 - 1\rangle + g_1 \sqrt{n_1} |b, n_1 - 1, n_2\rangle] .
\end{aligned} \tag{7}$$

We call these three dressed states, namely,  $|\psi_0(n_1, n_2)\rangle$ ,  $|\psi_{\pm}(n_1, n_2)\rangle$  as belonging to the  $(n_1, n_2)$ -photon sector. Thus the two-mode strong-coupling CQED with a  $V$ -type three-level atom enables the creation of tripartite superposition states involving the atom and the two quantized fields. The incoherent pumping and other incoherent processes such as spontaneous emission as well as classical drives will induce transitions to the states outside these three dressed states, thus coupling all other photon sectors. While dual incoherent pumping can lead to the enhancement of the excited-state population and the consequent lasing into the cavity modes, the coherent atomic drives can generate further coherence between the cavity-dressed states. This coherence plays an essential role in creating entanglement between two cavity modes. Furthermore, the coherent drives can lead to the amplification of the cavity modes without population inversion due to the coherence.

To keep the dressed-state analysis simple, we assume that  $\delta = 0$  and  $g_1 = g_2 = g$ ,  $\eta_{ic1} = \eta_{ic2} = \eta_{ic}$ ,  $\kappa_1 = \kappa_2 = \kappa$  and  $\gamma_1 = \gamma_2 = \gamma$ . The  $(0,0)$ -photon sector, that is when both the cavity fields are in vacuum, there exists only one joint state  $|a, 0, 0\rangle$ . Each of the  $(n_1, 0)$ - and  $(0, n_2)$ -photon sectors have two dressed states

$$\begin{aligned}
|\psi_{\pm}(n_1, 0)\rangle &= \frac{1}{\sqrt{2}} [|a, n_1, 0\rangle \pm |b, n_1 - 1, 0\rangle] , \\
|\psi_{\pm}(0, n_2)\rangle &= \frac{1}{\sqrt{2}} [|a, 0, n_2\rangle \pm |c, 0, n_2 - 1\rangle] .
\end{aligned} \tag{8}$$

The corresponding eigenvalues are  $\pm g$ . These are the familiar dressed states of two-state Jaynes-Cummings model. If the fields contain zero photon in one mode and a finite number of photons in the other mode, then in the absence of incoherent processes and any classical drive, the system effectively reduces to a two-level system. However, atomic drives and incoherent processes can connect  $\psi_{\pm}(n_1, 0)$  and  $\psi_{\pm}(0, n_2)$  to  $|a, n_1 - 1, 0\rangle$  and  $|a, 0, n_2 - 1\rangle$ , respectively. As we will show in the next section, when dual incoherent pumps are weak, that is,  $\eta_{ic} < (\kappa + \gamma)$ , the lasing actions and the nature of two-photon correlations between the generated photons can be interpreted in terms of an interplay between the coherent and incoherent transitions involving some low-lying bare or dressed states. For strong incoherent pumping  $\eta_{ic} \geq (\kappa + \gamma)$ , higher photon sectors get involved in the dynamics. The possible transitions between the bare states as well as between the dressed states belonging to a few low-lying photon sectors are schematically shown in Fig. 2



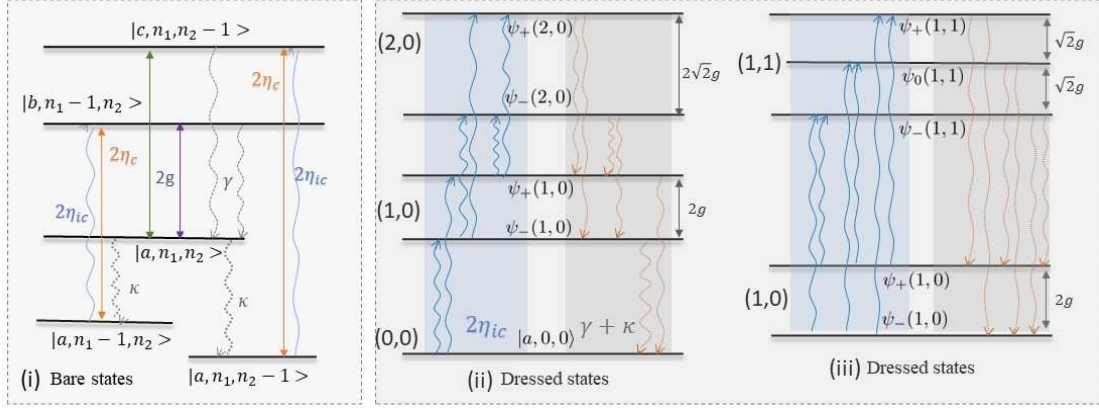


FIG. 2. (i) Bare-state level diagram with various transition pathways due to different incoherent processes and coherent atomic drives. (ii) and (iii) A few low lying dressed states with transitions due the incoherent processes only. Here  $g_1 = g_2 = g$  (atom-field coupling),  $\eta_{ic1} = \eta_{ic2} = \eta_{ic}$  (incoherent pumps) and  $\eta_{c1} = \eta_{c2} = \eta_c$  (coherent drives). In (i), the green and orange- double headed arrows represent the coherent couplings due to the cavity and driving fields, respectively. The curvy upward and downward arrows indicate incoherent pumping and atomic or cavity decay processes, respectively. In the dressed-state picture, the frequency spacing between the dressed states belonging to the same photon sector are marked. Note that the dressed-state diagram involving couplings among  $(0,0) \iff (0,1) \iff (0,2)$  is the same as in (ii) with ‘(1,0)’ and ‘(2,0)’ being replaced by ‘(0,1)’ and ‘(0,2)’, respectively. Similarly, the dressed-state diagram involving  $(0,1) \iff (1,1)$ , photon sectors will be same as in (iii) with ‘(1,0)’ being replaced by ‘(0,1)’. The spacing between different levels is not to be scaled.

### C. Incoherent pumping and damping

To include incoherent pumping and various damping processes in the system, we resort to the density matrix equation in Lindblad form

$$\frac{\partial \hat{\rho}_{sf}}{\partial t} = -\frac{i}{\hbar} [\mathcal{H}(\tilde{H}), \hat{\rho}_{sf}] + \sum_{i=1,2} \frac{\kappa_i}{2} \mathcal{L}_{a_i} + \sum_{j=1,2} \frac{\gamma_j}{2} \mathcal{L}_{\sigma_j} + \sum_{j=1,2} \frac{\eta_{icj}}{2} \mathcal{L}_{\sigma_j^\dagger}, \quad (9)$$

Where  $\rho_{sf}$  is the density matrix of joint system, comprising of the sub-system atom (denoted by ‘s’ and the cavity fields (denoted by ‘f’).  $\mathcal{L}_x$  is a Liouville super operator where  $x$  stands for any of the three operators  $a_i, \sigma_j^\dagger, \sigma_j$ .  $\kappa_i$  denotes the decay rate of the cavity field mode  $i$  ( $i = 1, 2$ ). Here



the Lindbladian superoperators

$$\begin{aligned}\mathcal{L}_{a_i} &= \left[ 2a_i\rho_{sf}a_i^\dagger - \left\{ a_i^\dagger a_i, \rho_{sf} \right\} \right] , \\ \mathcal{L}_{\sigma_j} &= \left[ 2\sigma_j\rho_{sf}\sigma_j^\dagger - \left\{ \sigma_j^\dagger \sigma_j, \rho_{sf} \right\} \right] ,\end{aligned}$$

describe the cavity and atomic damping, respectively; while

$$\mathcal{L}_{\sigma_j^\dagger} = \left[ 2\sigma_j^\dagger\rho_{sf}\sigma_j - \left\{ \sigma_j\sigma_j^\dagger, \rho_{sf} \right\} \right] , \quad (10)$$

describes incoherent pumping to the two upper levels of the atom. Here  $\{\alpha, \beta\}$  implies anticommutation between  $\alpha$  and  $\beta$ . The Liouvillian in Eq. (9) can also be expressed in a different form using the complex Hamiltonian

$$H_c = \mathcal{H} + i\hbar \sum_{i=1,2} \frac{\kappa_i}{2} a_i^\dagger a_i + i\hbar \sum_{j=1,2} \frac{\gamma_j}{2} \sigma_j^\dagger \sigma_j + i\hbar \sum_{j=1,2} \frac{\eta_{icj}}{2} \sigma_j \sigma_j^\dagger . \quad (11)$$

Explicitly, this form is

$$\frac{\partial \hat{\rho}_{sf}}{\partial t} = -\frac{i}{\hbar} [H_c \hat{\rho}_{sf} - \hat{\rho}_{sf} H_c^\dagger] + \sum_{i=1,2} \kappa_i a_i \rho_{sf} a_i^\dagger + \sum_{j=1,2} \left[ \gamma_j \sigma_j \rho_{sf} \sigma_j^\dagger + \eta_{icj} \sigma_j^\dagger \rho_{sf} \sigma_j \right] , \quad (12)$$

To numerically solve [54] the density matrix equation we use joint atom-field basis states  $|\alpha, n_1, n_2\rangle$  where  $\alpha$  denotes any of the three atomic states,  $n_1$  and  $n_2$  are the photon numbers. For a given set of system parameters, we first verify the convergence of our numerical results against the variation of the photon numbers in the two modes. Once we ensure the convergence, we truncate the Fock basis of the two fields for the chosen parameter set. We numerically obtain the steady-state solution of the joint atom-field density matrix.

#### D. Second-order photon-photon correlations and entanglement

We calculate the expectation value of an observable operator  $\hat{O}$  of interest in the steady-state by

$$\langle \hat{O} \rangle = \text{Tr} \left[ \hat{O} \hat{\rho}_{sf}^{ss} \right] = \sum_{\alpha} \sum_n \sum_m \langle \alpha, n, m | \hat{O} \hat{\rho}_{sf}^{ss} | \alpha, n, m \rangle .$$

where  $\alpha$  stands for an atomic state,  $n$  and  $m$  represent photon number states for mode 1 and 2, respectively. Here  $\hat{\rho}_{sf}^{ss} = \hat{\rho}_{sf}(t \rightarrow \infty)$  stands for the steady-state joint density matrix. If the operator  $\hat{O}$  describes only the atomic properties such as atomic population inversion or coherence,

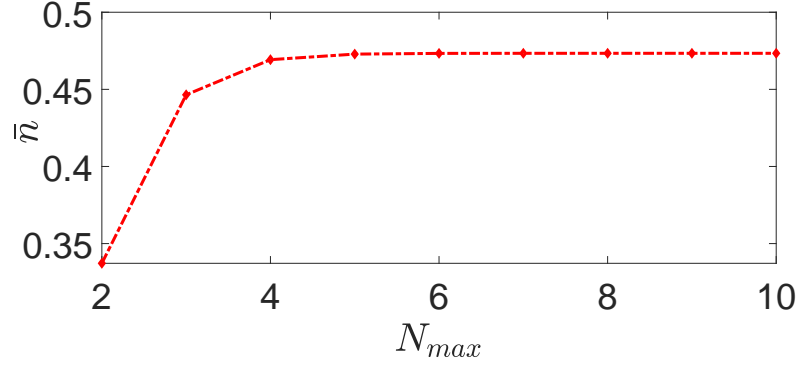


FIG. 3. The steady-state average photon numbers  $\bar{n}_1 = \bar{n}_2 = \bar{n}$ , as a function of the maximum Fock-state number ( $N_{max}$ ) in each mode considered for our calculations. The scaled atom-cavity coupling parameter is  $g_1 = g_2 = 10$ , the cavity damping rates are  $\kappa_1 = \kappa_2 = 1$  MHz, incoherent pump strengths are  $\eta_{ic1} = \eta_{ic2} = 2$  MHz and both modes are at resonance, i.e.,  $\delta_1 = \delta_2 = 0$ .

then one can use the reduced atomic density matrix to calculate the expectation value. The reduced atomic density matrix is given

$$\hat{\rho}_s = \text{Tr}_{\text{field}}[\hat{\rho}_{sf}] . \quad (13)$$

where  $\text{Tr}_{\text{field}}$  implies tracing over the two cavity field modes. The expectation value is then given by  $\langle \hat{O} \rangle = \text{Tr}_{\text{atom}} [\hat{O} \hat{\rho}_s]$ , where  $\text{Tr}_{\text{atom}}$  stands for tracing over the atomic states.

On the other hand, if  $\hat{O}$  refers to a field property only then we can use reduced two-mode field density matrix given by

$$\hat{\rho}_f = \text{Tr}_{\text{atom}}[\hat{\rho}_{sf}] . \quad (14)$$

Then the expectation value is given by  $\langle \hat{O} \rangle = \text{Tr}_{\text{field}} [\hat{O} \hat{\rho}_f]$ . We calculate the two-time Hanbury Brown-Twiss (HBT) second-order correlation function [55] as

$$g_{ij}^{(2)}(\tau) = \frac{\langle a_i^\dagger(t) a_j^\dagger(t+\tau) a_j(t+\tau) a_i(t) \rangle}{\langle a_i^\dagger(t) a_i(t) \rangle \langle a_j^\dagger(t+\tau) a_j(t+\tau) \rangle} . \quad (15)$$

where  $i = 1, 2$  and  $j = 1, 2$  denote the mode indexes. If  $i = j$  then we have intra-mode correlation, otherwise we obtain inter-mode correlation. Here  $\langle a_i^\dagger a_i \rangle$  is the mean photon number of the  $i^{\text{th}}$  cavity mode. Using quantum regression theorem [56–58], HBT function can be calculated for fluctuations around the steady state. Then we have

$$g_{ij}^{(2)}(\tau) = \frac{\text{Tr}_{\text{field}} [a_i^\dagger a_j^\dagger a_j a_i \rho_f(t \rightarrow \infty)]}{\text{Tr}_{\text{field}} [a_i^\dagger a_i \rho_f(t \rightarrow \infty)] \text{Tr}_{\text{field}} [a_j^\dagger a_j \rho_f(t \rightarrow \infty)]} . \quad (16)$$

For  $\tau \sim 0$ , the system's response manifests into photonic correlation ( $g_{ij}^{(2)}(0) > 1$ ) or anticorrelation ( $g_{ij}^{(2)}(0) < 1$ ). When  $g_{ij}^{(2)}(0) \gg 1$ , the photons are highly correlated in bunched form. i.e. bunching occurs. In contrast, when  $g_{ij}^{(2)}(0) < 1$ , there occurs photon antibunching and as  $g_{ij}^{(2)}(0) \rightarrow 0$ , the perfect photon blockade [6] takes place. Now, we define the frequency domain of correlation by Fourier transforming  $g_{ij}^{(2)}(\tau)$

$$\mathcal{F}_{ij}(\omega) = \int_{-\infty}^{\infty} [g_{ij}^{(2)}(\tau) - g_{ij}^{(2)}(\infty)] e^{i\omega\tau} d\tau. \quad (17)$$

Depending on the coherence in the system,  $g_{ij}^{(2)}(\tau)$  as a function of  $\tau$  may exhibit oscillatory behavior. In the limit  $\tau \rightarrow \infty$ ,  $g_{ij}^{(2)}(\tau) \rightarrow 1$ . To know the frequencies of the oscillations and other frequency-domain features of HBT correlations [59], it is important to study not only the time dependence of  $g_{ij}^{(2)}(\tau)$  but also the frequency dependence of  $\mathcal{F}_{ij}(\omega)$ . In the present context, the HBT correlations as a function of  $\tau$  will decay to the steady value of unity with a time constant  $\tau_d \sim (\kappa + \gamma)^{-1}$  while the oscillations will bear the signature of quantized Rabi dynamics.

Next, to explore the entanglement between the photons of the two cavity modes, we take partial transpose of Peres and Horodecki [60] over the mode 2 (or 1) of the two-mode reduced density matrix. The resulting matrix is denoted as  $\rho_f^{\text{PT},2}$  ( $\rho_f^{\text{PT},1}$ ). Partial transpose over field mode 2 implies that the basis operators of the bipartite density matrix change as  $|mn\rangle\langle\mu\nu| \rightarrow |m\nu\rangle\langle\mu n|$ . The negativity of at least one eigenvalue of  $\rho_f^{\text{PT},2}$  or ( $\rho_f^{\text{PT},1}$ ) implies that the two field modes are entangled.

### III. RESULTS AND DISCUSSIONS

To present and discuss the results in a systematic way, we first present the results in the absence of classical drives, and analyze the effects of the dual incoherent pumps. We then discuss the effects of coherent drives in the presence as well as in absence of incoherent pumps. Thus we clearly discern the effects of coherent drives from the incoherent pumps and vice versa.

For all our numerical results, we consider  $\gamma_1 = \gamma_2 = \gamma = 1$ , implying that we scale all the frequency quantities by  $\gamma$ .

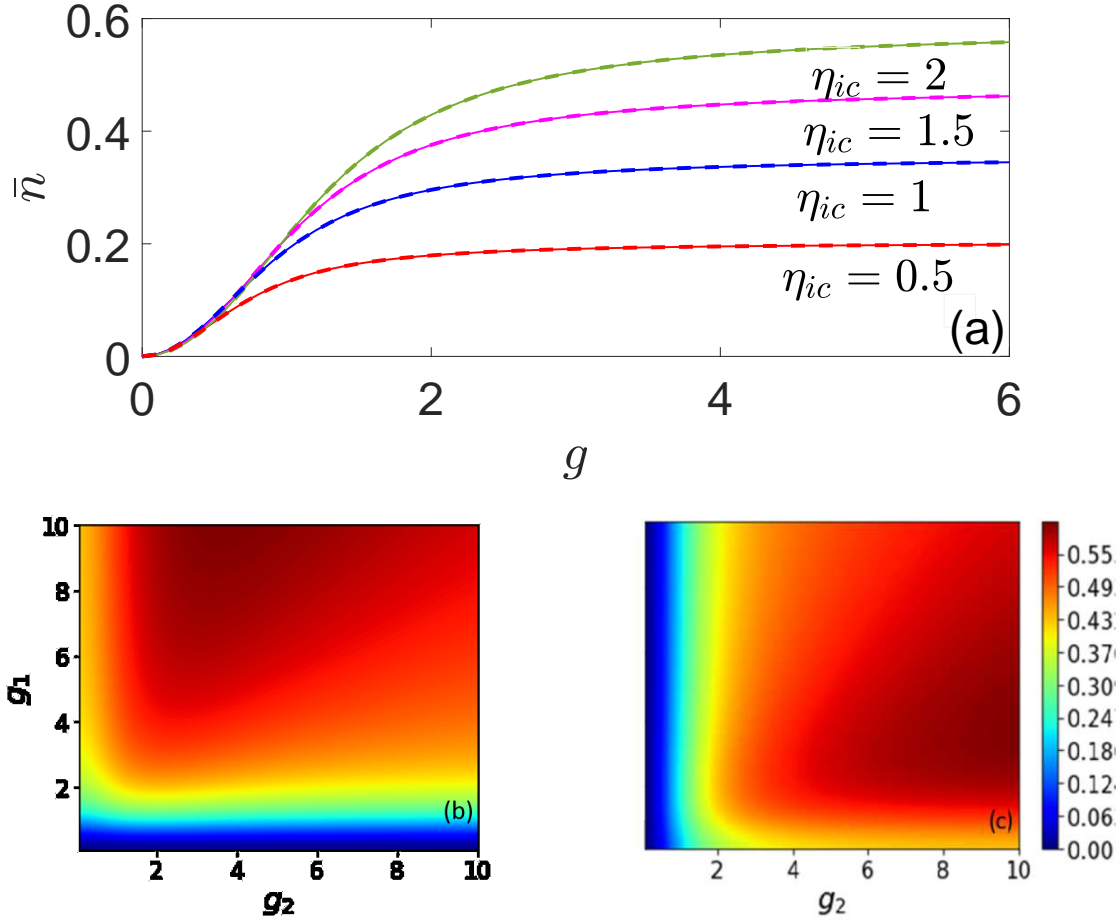


FIG. 4. (a) The average number of photons  $\bar{n}_1 = \bar{n}_2 = \bar{n}$  are plotted as a function of scaled atom-cavity coupling parameter  $g_1 = g_2 = g = 10$ . The other parameters are:  $\delta_1 = \delta_2 = 0$ ,  $\kappa_1 = \kappa_2 = 1$ ,  $\eta_{ic1} = \eta_{ic2} = 2, 1.5, 1, 0.5$ . The surface plots (b) and (c) depict the variation of  $\bar{n}_1$  (b) and  $\bar{n}_2$  (c) as a function of coupling parameters  $g_1$  and  $g_2$ , keeping  $\eta_{ic1} = \eta_{ic2} = 2$  with all other parameters remaining fixed.

#### A. The effects of incoherent pump only

First we consider the case when the three-level atom inside the cavity is pumped incoherently with no coherent drive being present. The level diagram with only incoherent couplings between the dressed states is schematically shown in Fig. 2 (ii) and (iii). Fig. 3 shows the convergence of the values of the average photon numbers  $\bar{n}_1 = \bar{n}_2 = \bar{n}$ , against the variation of the Fock basis size  $N_{max}$  for a chosen set of equal parameters for the two cavity modes. We find that the results converge for  $N_{max} \geq 5$  for the chosen parameter set as mentioned in the figure caption. For the

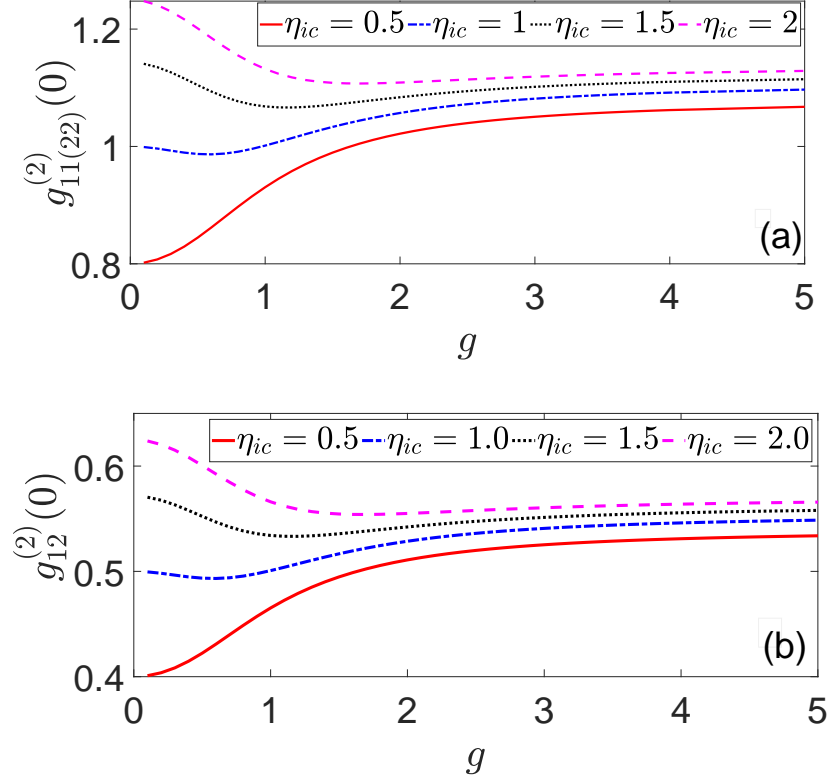


FIG. 5. (a) Equal-time intra-mode HBT correlation functions  $g_{11(22)}^{(2)}(0)$  and (b) inter-mode  $g_{12}^{(2)}(0)$  are plotted as a function of  $g$  for different incoherent pump strengths  $\eta_{ic} = 0.5$  (solid),  $\eta_{ic} = 1$  (dashed-dotted),  $\eta_{ic} = 1.5$  (dotted) and  $\eta_{ic} = 2$  (dashed). All other parameters are same as in Fig. 4 .

strong-coupling regime limited by  $g_1 \leq 10$  and  $g_2 \leq 10$ ; and  $\eta_{ic1} \leq 2$  and  $\eta_{ic2} \leq 2$ , we can safely restrict Fock states per cavity mode at  $N_{max} = 6$ . Throughout our analysis, we set  $N_{max} = 6$  for the two modes and do not take the value of  $g_1$  or  $g_2$  greater than 10 and that of  $\eta_{ic1}$  or  $\eta_{ic2}$  greater than 2.

Fig. 4 demonstrates that the dual incoherent pumping leads to the thresholdless two-mode lasing action. From Fig. 4(a), one can notice that as the atom-cavity coupling strengths  $g_1 = g_2 = g$  increase for equal and fixed incoherent pump strengths  $\eta_{ic1} = \eta_{ic2} = \eta_{ic}$  the average photon numbers  $\bar{n}_1 = \bar{n}_2 = \bar{n}$  first start growing and then saturate. Larger the value of  $\eta_{ic}$ , the larger is the saturation limit revealing that the dual incoherent pumping leads to amplification in both the modes. The surface plots in Fig. 4(b) and 4(c) show the variation of  $\bar{n}_1$  and  $\bar{n}_2$  against both  $g_1$  and  $g_2$ . These plots suggest that one can control the relative photon numbers in the two modes by changing the two atom-cavity coupling parameters. Below the saturation limit of  $g_i$  ( $i = 1, 2$ ),

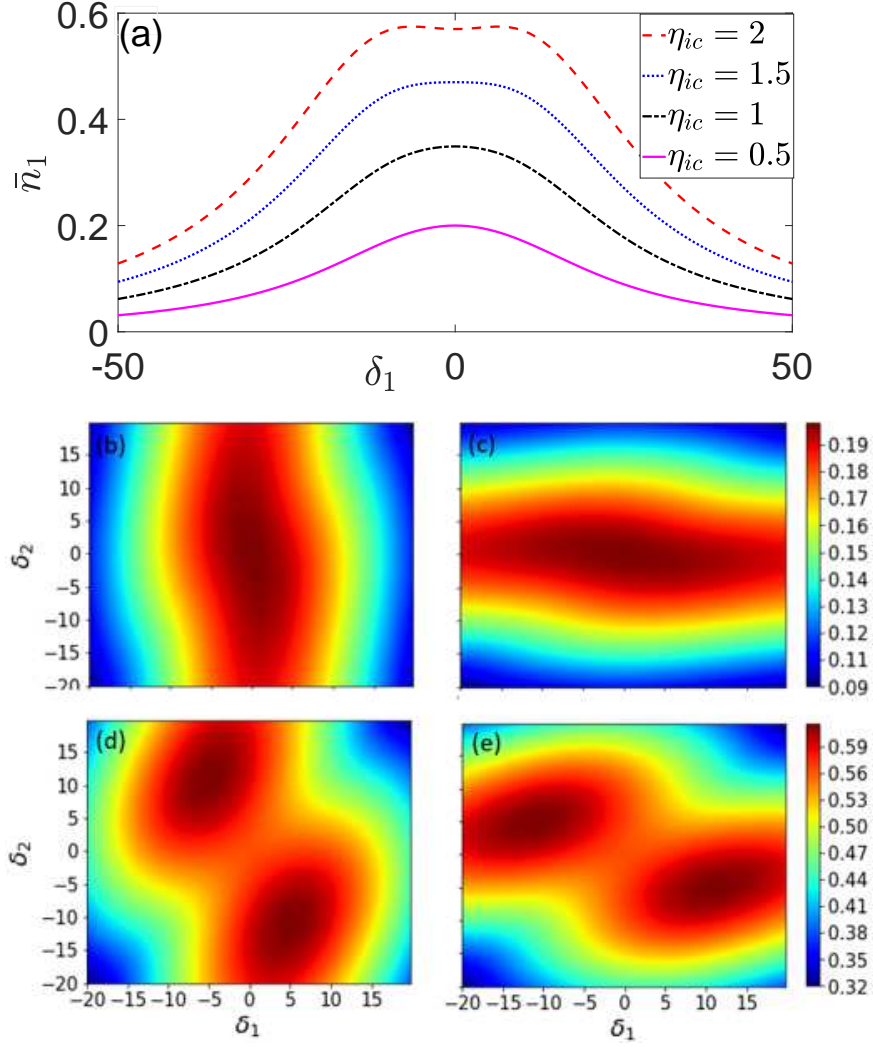


FIG. 6. (a)  $\bar{n}_1$  is plotted as a function of  $\delta_1$  for  $\eta_{ic} = 2$  (dashed),  $\eta_{ic} = 1.5$  (dotted),  $\eta_{ic} = 1$  (dashed-dotted),  $\eta_{ic} = 0.5$  (solid), for  $\delta_2 = 0$ ,  $g_1 = g_2 = 10$  and  $\kappa_1 = \kappa_2 = 1$ . The surface plots (b) and (c) exhibit the variation of  $\bar{n}_1$  and  $\bar{n}_2$ , respectively, as a function of both  $\delta_1$  and  $\delta_2$  for  $\eta_c = 0.5$ . The subplots (d) and (e) display the same as in (b) and (c), respectively, but for  $\eta_c = 2$ .

the average photon number in the  $i$ th mode is directly proportional to  $g_i$ . If we switch off one of the incoherent pumps, then the system reduces to an effective two-level atom pumped incoherently inside a single-mode cavity, leading to single-mode CQED laser.

In Fig. 5(a) equal-time Hanbury Brown-Twiss (HBT) intra-mode correlation function  $g_{11(22)}^{(2)}(0)$  is plotted against coupling parameter  $g_1 = g_2 = g$ , for four different values of  $\eta_{ic}$ : 0.5 (solid), 1.0 (dashed), 1.5 (dotted), 2 (dashed-dotted). If all other parameters corresponding to both the modes are equal, then  $g_{11}^{(2)}(0) = g_{22}^{(2)}(0)$ . Fig. 5(b) shows equal-time inter-mode HBT correlation func-

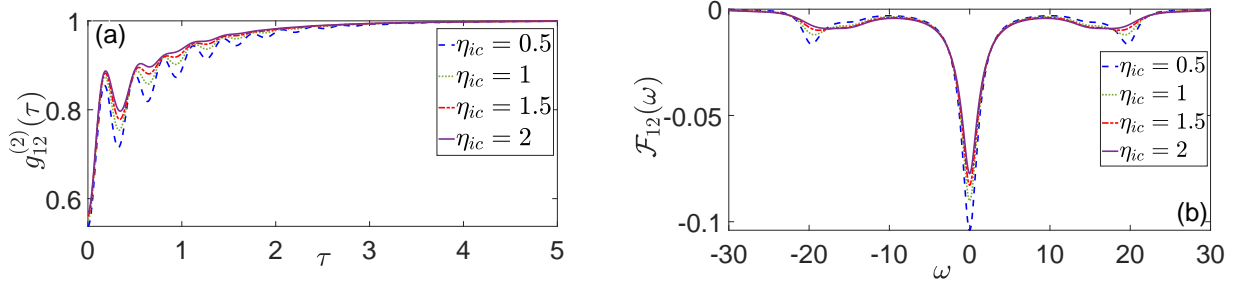


FIG. 7. (a) The inter-mode HBT correlation function  $g_{12}^{(2)}(\tau)$  is plotted against time-delay  $\tau$  and (b) the spectrum  $\mathcal{F}_{12}(\omega)$  of the correlation is plotted against frequency  $\omega$  for  $\eta_{ic} = 0.5$  (dashed),  $\eta_{ic} = 1$  (dotted),  $\eta_{ic} = 1.5$  (dashed-dotted),  $\eta_{ic} = 2$  (solid) keeping the light-matter coupling  $g_1 = g_2 = 10$  fixed. The rest of the parameters are same as in Fig. 4.

tion  $g_{12}^{(2)}(0)$  for the same parameters. For small values of  $\eta_{ic}$  and atom-cavity coupling constants being not very high, both inter and intra-mode HBT correlations show nonclassical behavior characterized by  $g_{11(22)}^{(2)}(0) < 1, g_{12}^{(2)}(0) < 1$ . As  $\eta_{ic}$  increases for fixed values of  $g$ , the inter-mode correlation remains nonclassical ( $g_{12}^{(2)}(0) < 1$ ), while the intra-mode correlation approaches thermal limit, i.e.,  $1 < g_{11(22)}^{(2)}(0) < 2$ . It is interesting to note that, the cavity photons of the same mode are most likely to appear in pairs, particularly for strong incoherent pumping. In contrast, if a photon in one mode is created in the case of weak incoherent pumping, a photon in the other mode can not be created at the same time. This feature may be explained from the point of view of an interplay between the coherent cavity-field Rabi dynamics and the incoherent processes as schematically depicted in the level diagram of Fig. 2. When the atom is initially in the ground state  $|a, 0, 0\rangle$  with the two cavity fields in the vacuum, the incoherent pumping can raise the atom to either of the excited states  $|b, 0, 0\rangle$  or  $|c, 0, 0\rangle$ . Suppose, the atom is excited to  $|b, 0, 0\rangle$ . Then the atom can either emit a photon in cavity mode 1 or into the vacuum by atomic decay. If it emits a photon into the cavity mode 1, then it will find itself in state  $|a, 1, 0\rangle$  until the photon leaks out of the cavity with the characteristic time scale  $\kappa^{-1}$ . In both the cases of atomic decay and cavity decay, the system will be reset to its initial state  $|a, 0, 0\rangle$ . Now, if the incoherent pumping strength is weak, then it is most likely that the system will be reset to its initial state rather than being promoted to the next higher photon sector. In the strong-coupling CQED regime with one photon in mode 1 and no photon in mode 2, there will be Rabi oscillations between the two atomic states  $|a\rangle$  and  $|b\rangle$  before the atom or the photon decays. Thus, for weak incoherent pumping, until



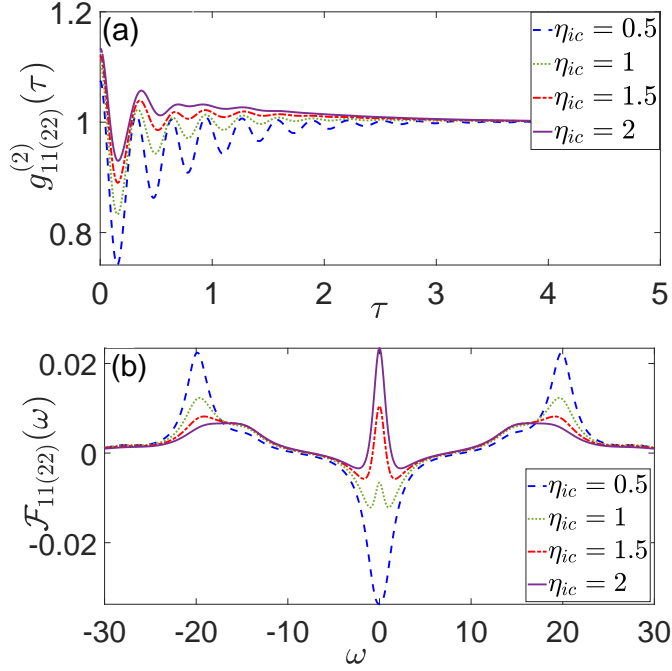


FIG. 8. (a) The intra-mode HBT functions  $g_{11}^{(2)}(\tau) = g_{22}^{(2)}(\tau)$  are plotted against time delay  $\tau$  and (b) the spectrum  $\mathcal{F}_{jj}(\omega)$  is plotted against frequency  $\omega$ , for  $\eta_{ic} = 0.5$  (dashed),  $\eta_{ic} = 1$  (dotted),  $\eta_{ic} = 1.5$  (dashed-dotted),  $\eta_{ic} = 2$  (solid) with  $g_1 = g_2 = 10$ . The rest of the parameters are the same as in Fig. 4.

and unless the atom is excited to  $|c, 0, 0\rangle$  from the reset state  $|a, 0, 0\rangle$  by incoherent processes, a photon in the mode 2 will not appear. This is the physical origin of the inter-mode photon-photon anti-bunching.

In Fig. 6(a), we plot  $\bar{n}_1$  vs.  $\delta_1$  for  $\delta_2 = 0$  for four different values of  $\eta_{ic}$  as mentioned in the legend of the figure. It is important to note that, as we increase  $\eta_{ic}$  above a certain value ( $\eta_{ic} \geq 1.5$ ), a single-peak structure is split into a double peak one. Figures 6(b) and 6(c) display the variation of  $\bar{n}_1$  and  $\bar{n}_2$ , respectively, as functions of both  $\delta_1$  and  $\delta_2$  for  $\eta_{ic} = 0.5$  while Fig. 6(d) and 6(e) show the same, respectively, for  $\eta_{ic} = 2$ . Figures 6(b) and 6(c) exhibit only one peak structure while Fig. 6(d) and 6(e) clearly show the two-peak structures. From these  $(\delta_1, \delta_2)$  plots, the positions of the two peaks for  $\bar{n}_1$  are detected to be  $(g/2, -\sqrt{2}g)$  and  $(-g/2, g)$  while those for  $\bar{n}_2$  are  $(\sqrt{2}g, -g/2)$  and  $(-g, g/2)$ , indicating that probably the lasing in the two modes occur due to stimulated transitions between the dressed state. For weak incoherent pumping, the amplification or lasing occurs primarily due to the transitions in the lower photon sectors, namely, (0,0)-, (1,0)- and (0,1)-sectors. In these sectors, the cavity-field stimulated transitions  $|b, 0, 0\rangle \rightarrow |a, 1, 0\rangle$

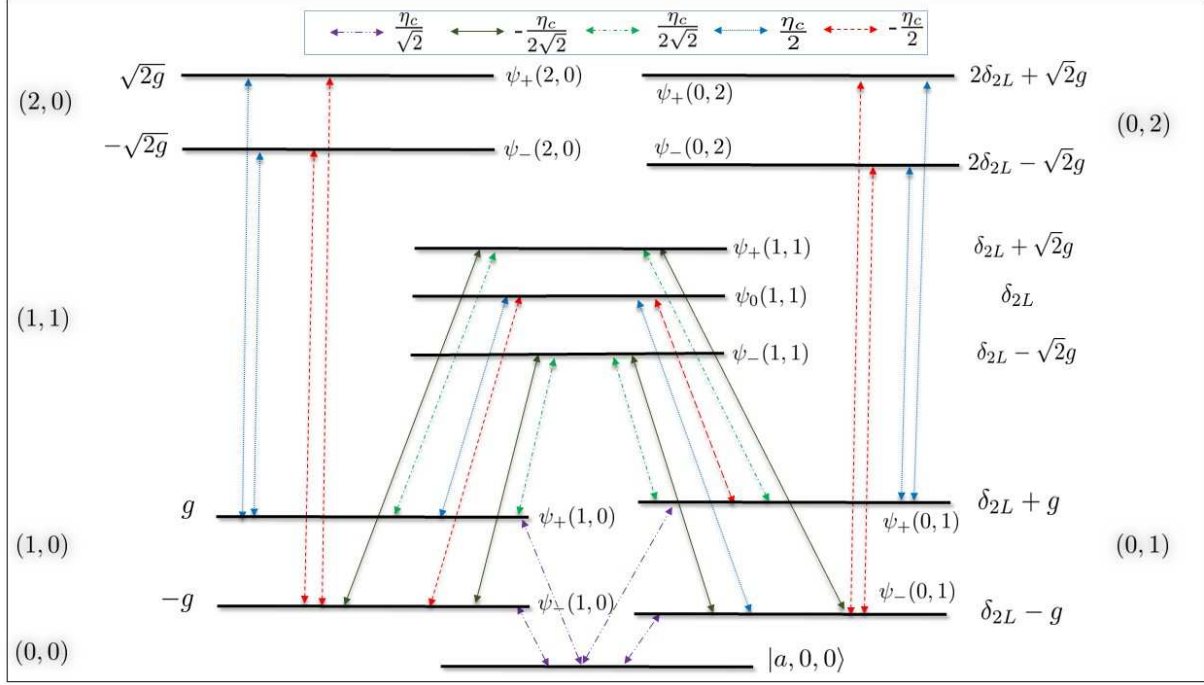


FIG. 9. Dressed-state level diagram showing couplings due to the coherent drives only for  $\eta_{c1} = \eta_{c2} = \eta_c$  and  $\delta = 0$ . The drives connect the dressed states from different photon sectors and the transition amplitude for each of the transitions is mentioned.

and  $|c, 0, 0\rangle \rightarrow |a, 0, 1\rangle$  to the two modes occur independently in two non-coupled two-level systems. The intensity of the emitted radiation is broadened due to strong CQED coupling giving the linewidth  $\sim 2g + \gamma + \kappa$  which is 22 for the parameters chosen. When incoherent pumping strength is increased beyond 1.5, the higher photon sectors (0,2),(2,0) becomes involved in the stimulated transition process. As shown in the bare- and dressed-state level diagram of Fig. 2, all three bare- or dressed-states become involved in the process for higher photon-sectors, leading to two-peak structure in the radiation intensity.

Fig. 7(a) shows the variation of  $g_{12}^{(2)}(\tau)$  against  $\tau$  while Fig. 7(b) exhibits the spectrum  $\mathcal{F}_{12}(\omega)$  as a function of frequency  $\omega$  for four different values of  $\eta_{ic}$  as mentioned in the legend. As  $\tau \rightarrow \infty$ ,  $g_{12}^{(2)}(\tau)$  reaches the value of unity implying that the two modes become uncorrelated in the long time delay limit. For low values of  $\eta_{ic}$ ,  $g_{12}^{(2)}(\tau)$  exhibits oscillatory decay from nonclassical domain ( $g_{12}^{(2)}(\tau) < 1$ ) towards coherent limit ( $g_{12}^{(2)}(\tau) \rightarrow 1$ ). As we increase  $\eta_{ic}$ , the amplitude of the oscillations gradually diminish. These oscillations are reminiscent of quantum beats and indicative of atomic coherence. The Fourier transform of  $g_{12}^{(2)}(\tau) - 1$ , that is,  $\mathcal{F}_{12}(\omega)$  as a function of  $\omega$  as

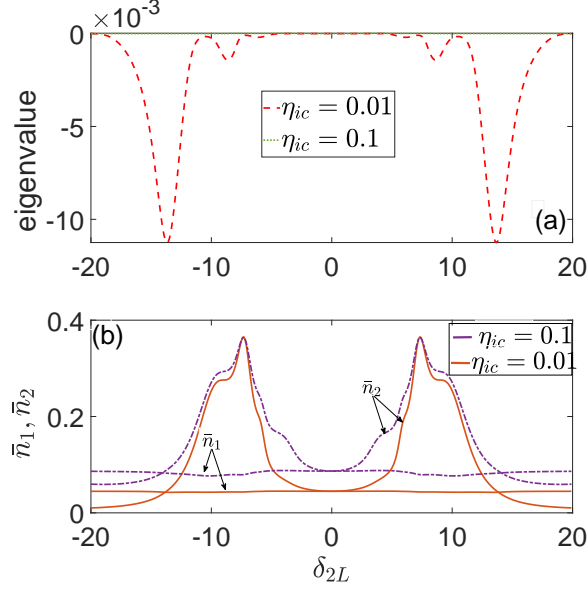


FIG. 10. (a) The smallest eigenvalue of  $\rho_f^{PT,2}$  is plotted against  $\delta_{2L}$ , for  $\eta_{ic} = 0.01$  (dotted),  $\eta_{ic} = 0.1$  (dashed). It shows the death of entanglement with the increase of incoherent pump strength  $\eta_{ic}$ . (b) average photon-number  $\bar{n}_2$  and  $\bar{n}_1$  vs.  $\delta_{2L}$  is plotted for  $\eta_{ic} = 0.01$  (solid),  $\eta_{ic} = 0.1$  (dashed-dotted). The rest of the parameters are  $g = 10, \kappa_1 = \kappa_2 = 1, \eta_{c1} = \eta_{c2} = \eta_c = 2$  and  $\delta_{1L} = 0$ .

shown in Fig. 7(b) reveals that there is one dominant frequency of oscillations which is  $2g$  in this case. We recall the vacuum-field Rabi splitting of two-level Jaynes-Cummings model is  $2g$ . This reveals that for low incoherent pumping, the photons are generated due to stimulated transitions in the (1,0)- and (0,1)-photon sectors. Remarkably, the anti-correlation between the two field modes  $g_{12}^{(2)}(\tau) - 1 < 0$  is also reflected in the  $\mathcal{F}_{12}(\omega)$  vs.  $\omega$  plots. This can be ascertained from the observation that the central peak of  $\mathcal{F}_{12}(\omega)$  at  $\omega = 0$  is negative. We have checked that as we gradually increase the strength of the incoherent pump, a new smaller dip appears at  $\omega = \sqrt{2}g$  in the  $\mathcal{F}_{12}(\omega)$  vs.  $\omega$  plot. The dressed-state energies of (1,1)-photon sector for  $\delta_1 = \delta_2 = 0$  are  $-\sqrt{2}g, 0$  and  $\sqrt{2}g$  and for (2,0) and (0,2) photon sectors it is  $\pm\sqrt{2}g$ . But (1,1) photon sector will not take part in this process as discussed in Eq. (19). This indicates that for relatively higher incoherent pump strength, the oscillations in the photon-photon correlations correspond to Rabi oscillations in these two-states CQED dynamics.

We display the variation of  $g_{11(22)}^{(2)}(\tau)$  as a function of  $\tau$  against in Fig. 8 (a) for four different values of  $\eta_{ic}$ . The correspond spectrum is shown in Fig. 8 (b). As in the case of inter-mode correlations, the intra-mode correlation too exhibits oscillatory decay. However, in contrast to

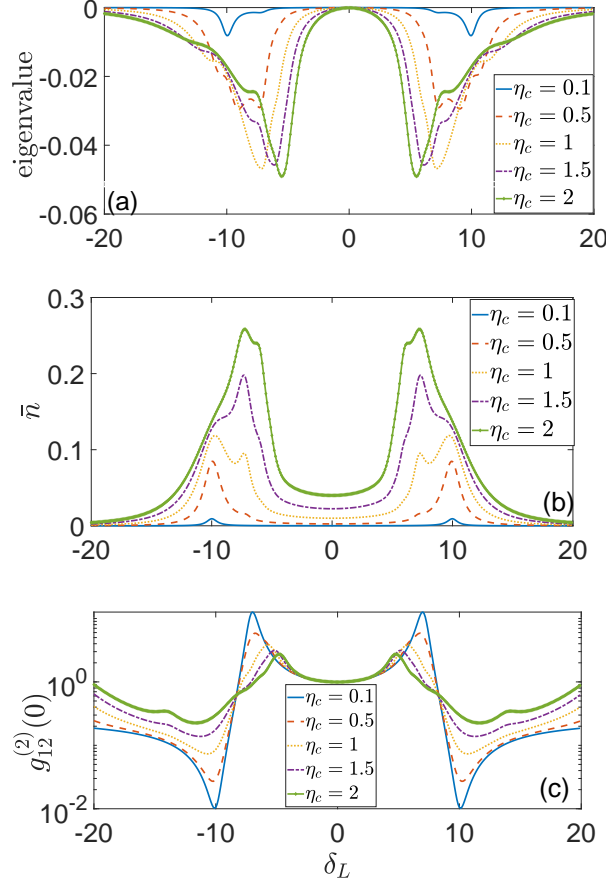


FIG. 11. The smallest eigenvalue of  $\rho_f^{1,2T}$  (a),  $\bar{n}_2 = \bar{n}_1 = \bar{n}$  (b) and  $g_{12}^{(2)}(0)$  (c) are plotted against  $\delta_{1L} = \delta_{2L} = \delta_L$  for  $\eta_c = 0.1$  (solid),  $\eta_c = 0.5$  (dashed),  $\eta_c = 1$  (dotted),  $\eta_c = 1.5$  (dashed-dotted) and  $\eta_c = 2$  (diamond marker). The rest of the parameters are same as in Fig. 10 with  $\eta_{ic} = 0$ .

inter-mode case, the intra-mode correlations become predominantly classical ( $g_{12}^{(2)}(\tau) \geq 1$ ) for  $\eta_{ic} > 1$  while they are mostly nonclassical for  $\eta_{ic} \leq 1$ . These correlation properties are also manifested in the spectral profiles in that the central peak of  $\mathcal{F}_{ii}(\omega)$  at  $\omega = 0$  is positive or negative for the classical or nonclassical correlations, respectively.

### B. The effects of coherent drives: Photon-Photon entanglement

Here we calculate the lowest eigenvalue of partially-transposed matrix of the reduced two-mode field density matrix as discussed in the subsection D of the previous section to verify the existence of photon-photon entanglement. The negativity of the eigenvalue is a clear signature

of the entanglement. For our chosen parameter regime and truncated Fock space, the reduced two-mode field density matrix is of  $36 \times 36$  dimension.

For simplicity, as before, we consider the two cavity fields are in two-photon resonance with the atomic transitions, that is,  $\delta_1 = \delta_2 = \delta$ . Under this condition, in a frame rotating with the driving laser frequencies, the eigenvalues of the three dressed states are given by

$$\begin{aligned} E_0/\hbar &= n_1\delta_{1L} + n_2\delta_{2L} - \delta, \\ E_{\pm}/\hbar &= n_1\delta_{1L} + n_2\delta_{2L} - \frac{\delta}{2} \pm \frac{1}{2}\sqrt{\delta^2 + 4(n_1g_1^2 + n_2g_2^2)}, \end{aligned}$$

where  $\delta_{1L} = \omega_1 - \omega_{1L} = \delta_1 + \Delta_b$  and  $\delta_{2L} = \omega_2 - \omega_{2L} = \delta_2 + \Delta_c$  are two cavity-drive detuning parameters. The dressed-state level diagram depicting the transitions due to the coherent drives that connect different photon sectors is shown in Fig. 9 for  $\eta_{c1} = \eta_{c2} = \eta_c$ . The amplitudes of the transitions are mentioned in the diagram. These transition amplitudes are given by

$$\langle \psi_{\alpha}(n_1, n_2) | \hbar\eta_c (\sigma_1 + \sigma_2 + \text{H.c.}) | \psi_{\beta}(n'_1, n'_2) \rangle. \quad (18)$$

where  $\alpha, \beta = 0, \pm$ ,  $|\psi_{\alpha}(n_1, n_2)\rangle$  and  $|\psi_{\beta}(n'_1, n'_2)\rangle$  refer to the dressed states as given by Eqs. 7 and 8. In the absence of incoherent pumping, as  $\eta_c$  increases from zero the coherent drives will couple from lower to higher dressed states successively as a consequence of the competition between the driving and the damping processes. The drives make superposition of the cavity-dressed states. The superposition state is an atom-field entangled state. Since the field is a two-mode one, if the atom is measured in a particular state, the atom-field entangled state will be projected into a two-mode entangled field state.

For numerical analysis of the effects of coherent drives, we set  $\kappa_1 = \kappa_2 = \kappa = 1$ ,  $\delta_1 = \delta_2 = 0$ ,  $g_1 = g_2 = 10$ . We plot the smallest eigenvalue of  $\rho_f^{\text{PT},2}$  against  $\delta_{2L}$  in Fig. 10(a) for  $\eta_{c1} = \eta_{c2} = \eta_c = 2$ ,  $\delta_{1L} = 0$  for two values of  $\eta_{ic}$ :  $\eta_{ic} = 0.01$  (dashed) and  $\eta_{ic} = 0.1$  (solid). Both the eigenvalues are negative though the magnitude is quite small ( $\sim 10^{-3}$ ). We notice that, for  $\eta_{ic} = 0.001$  the eigenvalue becomes appreciably negative while for  $\eta_{ic} = 0.1$  the magnitude of the eigenvalue is negligibly small ( $\sim 0$ ) compared to that for the former one. This implies that even a small increase of incoherent pump can destroy the entanglement. One can further notice that the eigenvalue for  $\eta_{ic} = 0.001$  has four dips: two at  $\delta_{2L} = \pm\sqrt{2}g$  and the other two at  $\delta_{2L} = g/\sqrt{2}$ . These dips correspond to the entangled states of the two-mode cavity fields. According to the dressed-state level diagram of Fig. 9,  $\delta_{2L} = \pm\sqrt{2}g$  corresponds to the shifts of the two dressed states  $|\psi^{\pm}(1, 1)\rangle$  in (1,1)-photon sector while  $\delta_{2L} = \pm g/\sqrt{2}$  corresponds to the shifts of the two

dressed states in (0,2)-photon sector. Since the value of  $\eta_{c1} = \eta_{c2} = 2$  is greater than the effective decay rate  $(\kappa + \gamma)/2 = 1$ , the atom is being relatively strongly driven in this case leading to the excitation of these higher level dressed states.

To know the average photon numbers in the two cavity modes when they are entangled, we plot both  $\bar{n}_2$  and  $\bar{n}_1$  as a function of  $\delta_{2L}$  in Fig. 10(b). The peaks in  $\bar{n}_2$  vs.  $\delta_{2L}$  plot at  $\delta_{2L} = \pm g$  correspond to vacuum-field Rabi splittings in the transitions between (0,0) and (0,1) photon sectors, while the two other peaks at  $\delta_{2L} = \pm g/\sqrt{2}$  correspond to one-photon Rabi splittings in the transitions between (0,1) and (0,2) photon sectors. We find that at  $\delta_{2L} = \pm\sqrt{2}g$ ,  $\bar{n}_1 \simeq \bar{n}_2 \simeq 0.05$ . In contrast at  $\delta_{2L} = \pm g/\sqrt{2}$ ,  $\bar{n}_1 \simeq 0.05$  and  $\bar{n}_2 \simeq 0.38$ . This means that the entangled states corresponding to  $\delta_{2L} = \pm g/\sqrt{2}$  have more number of photons in the second cavity mode due to resonant enhancement of the dressed states belonging to (0,2)- photon sector while the first cavity mode contains less number of photons as  $\delta_{1L} = 0$  corresponds to off-resonance due to the large shifts  $g/\sqrt{2} \simeq 7.1$ . The reason for the small number of photons in both the modes in the entangled states corresponding to  $\delta_{2L} = \pm\sqrt{2}g$  is the existence of the dark state  $|\psi_0(1,1)\rangle$  in the (1,1)-photon sector. The probability of photon emission into the two cavity modes is proportional to the quantity

$$|\langle \psi_\alpha(n_1, n_2) | [a_1^\dagger \sigma_1 + a_2^\dagger \sigma_2] | \psi_\beta(n_1, n_2) \rangle|^2. \quad (19)$$

For any two dressed states belonging to (1,1)-photon sector under two-photon resonance condition for the two cavity modes, the above quantity vanishes while it is finite for (1,0)-, (2,0)-, (0,1)- and (0,2)-photon sectors. This explains why there is small number of photons in the entangled states corresponding to  $\delta_{2L} = \pm\sqrt{2}g$ . Moreover,  $|\psi_0(1,1)\rangle$  can not be populated by the drives due to destructive interference between the transition pathways as schematically shown in Fig. 9.

Next we study the system driven by the dual coherent drives in the absence of any incoherent pump. The smallest eigenvalue of  $\rho_f^{\text{PT},2}$  as a function  $\delta_{2L} = \delta_{1L} = \delta_L$  is plotted in Fig. 11 (a). This figure shows that the eigenvalue becomes more negative with the increase of the coherent drive strength. Fig. 11(b) in  $\bar{n}_2, \bar{n}_1$  vs.  $\delta_L$  plots, the peak at  $\delta_L = g = 10$  corresponds to the emissions from (0,1),(1,0) photon sector. An additional peak appears at  $\delta_L = g/\sqrt{2} \simeq 7.1$  with the increase of  $\eta_c$  as a signature of the emission from (0,2),(2,0)-photon sector. Again, an emergence of another peak is observed at  $\delta_L = g/\sqrt{3} \simeq 6$  as an evidence of probing (2,1) and (1,2) photon sectors. Since both  $\bar{n}_1$  and  $\bar{n}_2$  are equal and appreciably enhanced, it is meaningful to analyse the statistical properties in this parameter regime. In Fig. 11 most of the dips in the negativity of the

eigenvalue correspond to the peaks in the photon number populations in both the modes as can be inferred by comparing Figs. 11 (a) with 11(b). In Fig. 11(c),  $g_{12}^{(2)}(0)$  is plotted as a function of  $\delta_L$ . It is to be noted that the inter-mode antibunching does not always necessarily mean inter-mode entanglement.

As mentioned before, the origin of the entanglement can be traced to the dressing of the cavity-dressed states by the coherent drives. The possibility of generating atom-photon entangled states, Schroedinger cat states of cavity fields and two-mode entangled field states by driving two-level atoms with a strong coherent field inside a single-mode cavity had been discussed by Solano, Agarwal and Walther [5] about two decades ago. They considered the dressed states of atoms due to the strong classical drive and then these atomic dressed states are then superposed by the cavity field, producing atom-cavity dressed states and thus leading to the entanglement. In our case, the two strong cavity fields first dress the three-level atom, leading to bimodal atom-cavity dressed states which are then further dressed by the coherent drives. Thus tripartite entangled states involving the atom and the two cavity modes are produced. Now, if the  $V$ -type three-level atom is measured in the ground state, the tripartite entangled state will be projected into a two-mode entangled field state. In fact, generation of two-mode entangled fields in the microwave frequency domain using a bimodal superconducting cavity and circular Rydberg atoms had been experimentally demonstrated by Heroche's group in 2001 [61]. In that experiment, the cavity was driven by excited Rydberg atoms that had passed through the cavity one by one. In 2005, Xiong, Scully and Zubairy [26] had theoretically shown that a "Correlated-spontaneous emission laser" using an ensemble of cascade or  $\Lambda$ -type three-level atoms driven by two classical coherent fields inside a doubly resonant cavity can produce two-mode entangled radiation with large number of photons in each mode.

#### IV. CONCLUSIONS

In conclusion, we have proposed a single-atom CQED laser that can generate nonclassically correlated and entangled photon pairs. We have shown that when the two cavity modes are incoherently pumped without any coherent drive, the laser produces amplified signals for both the modes with inter-mode nonclassical photon-photon correlation but with no photon-photon entanglement. The nonclassical behavior is manifested though inter-mode photon-photon anti-bunching which is shown to result from an interplay between the incoherent processes and cavity-field in-



duced coherent processes. When coherent atomic drives are used with small or no incoherent pumping, the laser generates inter-mode entangled photon pairs. We have demonstrated that the entanglement arises due to the dressing of the cavity-dressed states by the coherent drives. Our results show that increasing the incoherent pumping rates even by a small amount destroys the entanglement. As elaborated in our paper, not only the intensities of the generated fields, but also the photon-photon correlations and entanglement can be controlled at a microscopic level by varying the incoherent pumping rates, coherent drive strengths and detuning parameters, thus providing a wide range of functionality of our proposed laser system.

Our proposal may be implemented experimentally by combining the currently available technologies of cavity QED and atom traps. For example, an atom trap containing a single bosonic atom may be loaded inside a bimodal cavity. The three levels of the atom may be chosen in the following way: Let the atom in the ground electronic  $S$ -state be prepared in the hyperfine spin state  $|F, m_F = 0\rangle$ , where  $F$  is the hyperfine spin quantum number and  $m_F$  denotes the magnetic hyperfine spin quantum number. The two excited ( $P$ ) states be represented by  $|F', m'_F = -1\rangle$  and  $|F', m'_F = 1\rangle$ , where the excited hyperfine spin  $F' \geq 1$ . Now, if the two cavity modes are chosen to be left and right circularly polarized fields then our proposed one-atom laser will produce polarization-entangled photon pairs with antibunching. This may be realized with a doubly resonant cavity for which the two cavity axes for the two modes may coincide as shown in Fig. 1 (ii). As regards the implementation of incoherent optical pumping, Kimble's group at Cal-tech has already experimentally demonstrated such pumping in CQED using incoherent Raman transitions in a single-atom far-off resonance trap (FORT) loaded inside a cavity [62]. In the single-mode CQED laser with a single trapped Cs atom reported in Ref. [37], the laser output was available for a short duration limited by the lifetime of the trap which was 50 ms. This time limitation may be overcome by using single-ion trap instead of a single-atom trap in CQED regime [36, 63]. Because, the lifetime of an ion-trap is quite large. Furthermore, an ion trap may offer some advantages as far as coherent or incoherent optical pumping is concerned as the stability of an ion-trap does not depend on the internal electronic states of the ion unlike that of an atom-trap. Therefore, ion-trap CQED may be an interesting research direction for generating nonclassical and entangled photon pairs for practical applications.

---

[1] P. R. Berman, Ed., *Cavity quantum electrodynamics* (Academic Press, San Diego, CA, 1994).

- [2] H. Walther, B. T. H. Varcoe, B.-G. Englert, and T. Becker, [Reports on Progress in Physics](#) **69**, 1325 (2006).
- [3] R. Miller, T. E. Northup, K. M. Birnbaum, A. Boca, A. D. Boozer, and H. J. Kimble, [Journal of Physics B: Atomic, Molecular and Optical Physics](#) **38**, S551 (2005).
- [4] J. M. Raimond, M. Brune, and S. Haroche, [Rev. Mod. Phys.](#) **73**, 565 (2001).
- [5] E. Solano, G. S. Agarwal, and H. Walther, [Phys. Rev. Lett.](#) **90**, 027903 (2003).
- [6] A. Imamoglu, H. Schmidt, G. Woods, and M. Deutsch, [Phys. Rev. Lett.](#) **79**, 1467 (1997).
- [7] K. M. Birnbaum, A. Boca, R. Miller, A. D. Boozer, T. E. Northup, and H. J. Kimble, [Nature](#) **436**, 87 (2005).
- [8] C. J. Zhu, Y. P. Yang, and G. S. Agarwal, [Phys. Rev. A](#) **95**, 063842 (2017).
- [9] C. J. Villas-Boas, K. N. Tolazzi, B. Wang, C. Ianzano, and G. Rempe, [Phys. Rev. Lett.](#) **124**, 093603 (2020).
- [10] S. L. Mielke, G. T. Foster, and L. A. Orozco, [Phys. Rev. Lett.](#) **80**, 3948 (1998).
- [11] M. Koch, C. Sames, M. Balbach, H. Chibani, A. Kubanek, K. Murr, T. Wilk, and G. Rempe, [Phys. Rev. Lett.](#) **107**, 023601 (2011).
- [12] M. Li, C.-L. Zou, D. Liu, G.-P. Guo, G.-C. Guo, and X.-F. Ren, [Phys. Rev. A](#) **98**, 012121 (2018).
- [13] D. G. England, B. Balaji, and B. J. Sussman, [Phys. Rev. A](#) **99**, 023828 (2019).
- [14] F. Hudelist, J. Kong, C. Liu, J. Jing, Z. Y. Ou, and W. Zhang, [Nature Communications](#) **5**, 3049 (2014).
- [15] K. A. Forbes, J. S. Ford, and D. L. Andrews, [Phys. Rev. Lett.](#) **118**, 133602 (2017).
- [16] X.-W. Xu, H.-Q. Shi, J.-Q. Liao, and A.-X. Chen, [Phys. Rev. A](#) **100**, 053802 (2019).
- [17] H. Xiong, M. O. Scully, and M. S. Zubairy, [Phys. Rev. Lett.](#) **94**, 023601 (2005).
- [18] J. Hinney, A. S. Prasad, S. Mahmoodian, K. Hammerer, A. Rauschenbeutel, P. Schneeweiss, J. Volz, and M. Schemmer, [Phys. Rev. Lett.](#) **127**, 123602 (2021).
- [19] T. F. Langerfeld, H. M. Meyer, and M. Köhl, [Phys. Rev. A](#) **97**, 023822 (2018).
- [20] C. K. Hong, Z. Y. Ou, and L. Mandel, [Phys. Rev. Lett.](#) **59**, 2044 (1987).
- [21] P. G. Kwiat, K. Mattle, H. Weinfurter, A. Zeilinger, A. V. Sergienko, and Y. Shih, [Phys. Rev. Lett.](#) **75**, 4337 (1995).
- [22] J.-W. Pan, Z.-B. Chen, C.-Y. Lu, H. Weinfurter, A. Zeilinger, and M. Żukowski, [Rev. Mod. Phys.](#) **84**, 777 (2012).
- [23] M. Müller, S. Bounouar, K. D. Jöns, M. Glässl, and P. Michler, [Nature Photonics](#) **8**, 224 (2014).
- [24] Y. Ren, S. Duan, W. Xie, Y. Shao, and Z. Duan, [Phys. Rev. A](#) **103**, 053710 (2021).

- [25] J. P. Clemens, P. R. Rice, P. K. Rungta, and R. J. Brecha, [Phys. Rev. A \*\*62\*\*, 033802 \(2000\)](#).
- [26] H. Xiong, M. O. Scully, and M. S. Zubairy, [Phys. Rev. Lett. \*\*94\*\*, 023601 \(2005\)](#).
- [27] S. Qamar, F. Ghafoor, M. Hillery, and M. S. Zubairy, [Phys. Rev. A \*\*77\*\*, 062308 \(2008\)](#).
- [28] A.-p. Fang, Y.-l. Chen, F.-l. Li, H.-r. Li, and P. Zhang, [Phys. Rev. A \*\*81\*\*, 012323 \(2010\)](#).
- [29] A. Devi, S. D. Gunapala, and M. Premaratne, [Phys. Rev. A \*\*105\*\*, 013701 \(2022\)](#).
- [30] Y. Mu and C. M. Savage, [Phys. Rev. A \*\*46\*\*, 5944 \(1992\)](#).
- [31] T. Pellizzari and H. Ritsch, [Journal of Modern Optics \*\*41\*\*, 609 \(1994\)](#).
- [32] M. Löffler, G. M. Meyer, and H. Walther, [Phys. Rev. A \*\*55\*\*, 3923 \(1997\)](#).
- [33] J. McKeever, A. Boca, A. D. Boozer, R. Miller, J. R. Buck, A. Kuzmich, and H. J. Kimble, [Science \*\*303\*\*, 1992 \(2004\)](#).
- [34] M. Khajavikhan, A. Simic, M. Katz, J. H. Lee, B. Slutsky, A. Mizrahi, V. Lomakin, and Y. Fainman, [Nature \*\*482\*\*, 204 \(2012\)](#).
- [35] G. S. Agarwal and S. Dutta Gupta, [Phys. Rev. A \*\*42\*\*, 1737 \(1990\)](#).
- [36] G. M. Meyer, H.-J. Briegel, and H. Walther, [Europhysics Letters \*\*37\*\*, 317 \(1997\)](#).
- [37] J. McKeever, A. Boca, A. D. Boozer, J. R. Buck, and H. J. Kimble, [Nature \*\*425\*\*, 268 \(2003\)](#).
- [38] A. D. Boozer, A. Boca, J. R. Buck, J. McKeever, and H. J. Kimble, [Phys. Rev. A \*\*70\*\*, 023814 \(2004\)](#).
- [39] P. Filipowicz, J. Javanainen, and P. Meystre, [Phys. Rev. A \*\*34\*\*, 3077 \(1986\)](#).
- [40] L. Davidovich, J. M. Raimond, M. Brune, and S. Haroche, [Phys. Rev. A \*\*36\*\*, 3771 \(1987\)](#).
- [41] G. Rempe, F. Schmidt-Kaler, and H. Walther, [Phys. Rev. Lett. \*\*64\*\*, 2783 \(1990\)](#).
- [42] M. Weidinger, B. T. H. Varcoe, R. Heerlein, and H. Walther, [Phys. Rev. Lett. \*\*82\*\*, 3795 \(1999\)](#).
- [43] F. De Martini, F. Cairo, P. Mataloni, and F. Verzeqnessi, [Phys. Rev. A \*\*46\*\*, 4220 \(1992\)](#).
- [44] K. An, J. J. Childs, R. R. Dasari, and M. S. Feld, [Phys. Rev. Lett. \*\*73\*\*, 3375 \(1994\)](#).
- [45] V. V. Kozlov, Y. Rostovtsev, and M. O. Scully, [Phys. Rev. A \*\*74\*\*, 063829 \(2006\)](#).
- [46] S. Barnett and P. M. Radmore, *Methods in theoretical quantum optics* (Oxford University Press, New York, 1997).
- [47] A. Pal and B. Deb, [Optics Communications \*\*431\*\*, 1 \(2019\)](#).
- [48] C. Liu, Z. Dutton, C. H. Behroozi, and L. V. Hau, [Nature \*\*409\*\*, 490 \(2001\)](#).
- [49] E. Arimondo, *Coherent Population Trapping in Laser Spectroscopy*, edited by E. Wolf, Progress in Optics, Vol. 35 (Elsevier, 1996) pp. 257–354.
- [50] M. O. Scully, [Phys. Rev. Lett. \*\*55\*\*, 2802 \(1985\)](#).
- [51] M. O. Scully, G. Süssmann, and C. Benkert, [Phys. Rev. Lett. \*\*60\*\*, 1014 \(1988\)](#).

- [52] M. O. Scully and M. S. Zubairy, [Phys. Rev. A \*\*35\*\*, 752 \(1987\)](#).
- [53] S.-Y. Zhu and M. O. Scully, [Phys. Rev. A \*\*38\*\*, 5433 \(1988\)](#).
- [54] J. Johansson, P. Nation, and F. Nori, [Computer Physics Communications \*\*184\*\*, 1234 \(2013\)](#).
- [55] C. Jurczak, K. Sengstock, R. Kaiser, N. Vansteenkiste, C. Westbrook, and A. Aspect, [Optics Communications \*\*115\*\*, 480 \(1995\)](#).
- [56] M. Lax, [Phys. Rev. \*\*129\*\*, 2342 \(1963\)](#).
- [57] M. Lax, [Phys. Rev. \*\*157\*\*, 213 \(1967\)](#).
- [58] H. J. Carmichael, *Statistical methods in quantum optics I* (Springer-Verlag, Berlin, 1999).
- [59] K. Adhikary, A. Dey, A. Pal, S. Mal, and B. Deb, [Phys. Rev. A \*\*103\*\*, 033310 \(2021\)](#).
- [60] A. Peres, [Phys. Rev. Lett. \*\*77\*\*, 1413 \(1996\)](#).
- [61] A. Rauschenbeutel, P. Bertet, S. Osnaghi, G. Nogues, M. Brune, J. M. Raimond, and S. Haroche, [Phys. Rev. A \*\*64\*\*, 050301 \(2001\)](#).
- [62] D. Boozer, [Raman Transitions in Cavity QED](#) (Dissertation (Ph.D.), California Institute of Technology, 2005).
- [63] B. Casabone, K. Friebe, B. Brandstätter, K. Schüppert, R. Blatt, and T. E. Northup, [Phys. Rev. Lett. \*\*114\*\*, 023602 \(2015\)](#).